On the Order of Accuracy and Numerical Performance of Two Classes of Finite Volume WENO Schemes

Rui Zhang[1], Mengping Zhang[1] and Chi-Wang Shu[2,*]

[1] *Department of Mathematics, University of Science and Technology of China, Hefei, Anhui 230026, China.*
[2] *Division of Applied Mathematics, Brown University, Providence, RI 02912, USA.*

Dedicated to the memory of Professor David Gottlieb

Abstract. In this paper we consider two commonly used classes of finite volume weighted essentially non-oscillatory (WENO) schemes in two dimensional Cartesian meshes. We compare them in terms of accuracy, performance for smooth and shocked solutions, and efficiency in CPU timing. For linear systems both schemes are high order accurate, however for nonlinear systems, analysis and numerical simulation results verify that one of them (Class A) is only second order accurate, while the other (Class B) is high order accurate. The WENO scheme in Class A is easier to implement and costs less than that in Class B. Numerical experiments indicate that the resolution for shocked problems is often comparable for schemes in both classes for the same building blocks and meshes, despite of the difference in their formal order of accuracy. The results in this paper may give some guidance in the application of high order finite volume schemes for simulating shocked flows.

1 Introduction and the setup of the schemes

In this paper we are interested in numerically solving two dimensional conservation law systems

$$u_t + f(u)_x + g(u)_y = 0 \tag{1.1}$$

Corresponding author. Email addresses: `rui@ustc.edu.cn` (R. Zhang), `mpzhang@ustc.edu.cn` (M. Zhang), `shu@dam.brown.edu` (C.-W. Shu)

with suitable initial and boundary conditions, using the finite volume schemes on Cartesian meshes. For this purpose, the computational domain is decomposed to rectangular cells

$$\Omega_{ij} = [x_{i-1/2}, x_{i+1/2}] \times [y_{j-1/2}, y_{j+1/2}],$$

and for simplicity we assume the mesh sizes $\Delta x = x_{i+1/2} - x_{i-1/2}$ and $\Delta y = y_{j+1/2} - y_{j-1/2}$ are constants. This assumption is not essential: finite volume schemes in this paper can be defined on arbitrary Cartesian meshes, even those with abrupt changes in mesh sizes, without affecting their conservation, accuracy and stability, in contrast to high order conservative finite difference schemes which can only be defined on smooth meshes. Finite volume schemes are also easier to implement in an adaptive mesh environment, for example in the AMR type schemes (e.g., [18]). This is the main reason that high order finite volume schemes are still commonly used in practice, even though high order finite difference schemes are much less expensive in multi-dimensions in uniform or smooth Cartesian meshes, see for example [3] for a comparison of finite volume and finite difference schemes in the context of essentially non-oscillatory (ENO) reconstructions.

In a finite volume scheme we seek approximations to the cell averages

$$\bar{\bar{u}}_{i,j} = \frac{1}{\Delta x \Delta y} \int_{y_{j-\frac{1}{2}}}^{y_{j+\frac{1}{2}}} \int_{x_{i-\frac{1}{2}}}^{x_{i+\frac{1}{2}}} u(x,y) dx dy. \tag{1.2}$$

We use the notation $\bar{u}$ to denote the cell averaging operation in the x-direction (integral in the cell $[x_{i-1/2}, x_{i+1/2}]$ divided by the cell size Δx), and $\tilde{u}$ to denote the cell averaging operation in the y-direction. The two dimensional cell average $\bar{\bar{u}}$ can be obtained by successively performing the cell averaging operators in x and in y. If we integrate the conservation law (1.1) over the cell Ω_{ij} and then divide by its area, we obtain

$$\frac{d\bar{\bar{u}}_{i,j}}{dt} + \frac{1}{\Delta x} \left(\tilde{f}_{i+\frac{1}{2},j} - \tilde{f}_{i-\frac{1}{2},j} \right) + \frac{1}{\Delta y} \left(\bar{g}_{i,j+\frac{1}{2}} - \bar{g}_{i,j-\frac{1}{2}} \right) = 0, \tag{1.3}$$

where $\bar{\bar{u}}_{i,j}$ is the cell average (1.2) and

$$\tilde{f}_{i+\frac{1}{2},j} = \frac{1}{\Delta y} \int_{y_{j-\frac{1}{2}}}^{y_{j+\frac{1}{2}}} f\left(u(x_{i+\frac{1}{2}}, y) \right) dy, \tag{1.4a}$$

$$\bar{g}_{i,j+\frac{1}{2}} = \frac{1}{\Delta x} \int_{x_{i-\frac{1}{2}}}^{x_{i+\frac{1}{2}}} g\left(u(x, y_{j+\frac{1}{2}}) \right) dx \tag{1.4b}$$

are the physical fluxes, which are cell averages of $f(u)$ in y at $x = x_{i+1/2}$ and of $g(u)$ in x at $y = y_{j+1/2}$ respectively. Although (1.3) looks like a scheme, we should emphasize that it is actually an equality satisfied by the exact solution of the PDE (1.1).

Notice that the equality (1.3) describes the evolution of the cell averages $\bar{\bar{u}}_{i,j}$ while requiring the information of point values of the solution u in evaluating the physical fluxes in (1.4a) and (1.4b). In order to convert the equality (1.3) to a scheme (commonly

referred to as a finite volume scheme, since it solves for the cell averages $\bar{\bar{u}}_{i,j}$ rather than point values of the solution) in the following form

$$\frac{d\bar{\bar{u}}_{i,j}}{dt} + \frac{1}{\Delta x}\left(\hat{f}_{i+\frac{1}{2},j} - \hat{f}_{i-\frac{1}{2},j}\right) + \frac{1}{\Delta y}\left(\hat{g}_{i,j+\frac{1}{2}} - \hat{g}_{i,j-\frac{1}{2}}\right) = 0, \tag{1.5}$$

we must use a *reconstruction procedure* to obtain the approximate fluxes $\hat{f}_{i+1/2,j}$ and $\hat{g}_{i,j+1/2}$ in (1.5) as accurate approximations to the physical fluxes $\tilde{f}_{i+1/2,j}$ and $\bar{g}_{i,j+1/2}$ in (1.4a) and (1.4b).

We consider two classes of finite volume schemes in this paper. Both of them depend crucially on the following one-dimensional reconstruction procedure.

One-dimensional reconstruction procedure

Given the cell averages

$$\bar{u}_i = \frac{1}{\Delta x}\int_{x_{i-\frac{1}{2}}}^{x_{i+\frac{1}{2}}} u(x)dx$$

of a piecewise smooth function $u(x)$, the procedure uses these cell averages in several neighboring cells $\bar{u}_{i-\ell}, \cdots, \bar{u}_{i+k}$ (the collection of these neighboring cells is referred to as the *stencil* of the reconstruction) to obtain an approximation to the point value $u(x_{i+1/2})$ at the cell interface or at another point $u(x^*)$ where x^* is in the cell $[x_{i-1/2}, x_{i+1/2}]$. We require the reconstruction to be high order accurate when $u(x)$ is smooth in the stencil, and to be essentially non-oscillatory near discontinuities.

Such reconstruction procedure has been extensively studied in the literature, among high order ones we mention the essentially non-oscillatory (ENO) reconstruction [6] and the weighted ENO (WENO) reconstruction [8,9]. In the appendix we list the fifth order WENO reconstruction procedure [8] that we use in this paper. More details about WENO reconstruction can be found in, e.g., [10,13,14]. Further development of ENO and WENO schemes can be found, in, e.g., [2,7,12].

For a given physical flux $f(u)$, based on monotonicity in the scalar case and on characteristic information and Riemann solvers in the system case, we can define a numerical flux $\hat{f}(u^-, u^+)$ where u^- and u^+ approximate the left and right limits of the function u respectively. The numerical flux $\hat{f}(u^-, u^+)$ is at least Lipschitz continuous for both arguments, and is consistent with the physical flux in the sense that $\hat{f}(u, u) = f(u)$. Examples of numerical fluxes for systems of conservation laws in fluid dynamics can be found in, e.g., [11,16]. In this paper we use the Lax-Friedrichs flux and the HLLC flux as representative examples.

In the construction of finite volume schemes we often need to use a q-point Gaussian quadrature to approximate line integrals such as those in (1.4a) and (1.4b):

$$\tilde{f}_{i+\frac{1}{2},j} \approx \sum_{k=1}^{q} \beta_k f\left(u(x_{i+\frac{1}{2}}, y_j^k)\right), \qquad \bar{g}_{i,j+\frac{1}{2}} \approx \sum_{k=1}^{q} \beta_k g\left(u(x_i^k, y_{j+\frac{1}{2}})\right), \tag{1.6}$$

where β_k are the Gaussian quadrature weights, and y_j^k and x_i^k are the Gaussian quadrature points. In this paper we consider only schemes up to fifth order accuracy, hence $q=3$ suffices.

We are now ready to define the two classes of finite volume schemes that we will study in this paper. The first class (Class A) of these methods has the following algorithm flowchart:

Finite volume scheme, Class A

1. Using the two dimensional cell averages $\bar{\bar{u}}_{i,j}$, perform a one-dimensional reconstruction procedure in y to obtain a high order accurate approximation to the cell average of u in x at $y=y_{j+1/2}$, denoted by $\bar{u}_{i,j+1/2}$. For the purpose of upwinding and stability, typically two different approximations, denoted by $\bar{u}_{i,j+1/2}^-$ and $\bar{u}_{i,j+1/2}^+$, based on stencils biased to the left and to the right respectively, are obtained.

2. Using the two dimensional cell averages $\bar{\bar{u}}_{i,j}$, perform a one-dimensional reconstruction procedure in x to obtain a high order accurate approximation to the cell average of u in y at $x=x_{i+1/2}$, denoted by $\tilde{u}_{i+1/2,j}$. Again, two different approximations, denoted by $\tilde{u}_{i+1/2,j}^-$ and $\tilde{u}_{i+1/2,j}^+$, based on stencils biased to the left and to the right respectively, are obtained.

3. Form the approximate fluxes simply as

$$\hat{f}_{i+\frac{1}{2},j} = \hat{f}\left(\tilde{u}_{i+\frac{1}{2},j}^-, \tilde{u}_{i+\frac{1}{2},j}^+\right), \qquad \hat{g}_{i,j+\frac{1}{2}} = \hat{g}\left(\bar{u}_{i,j+\frac{1}{2}}^-, \bar{u}_{i,j+\frac{1}{2}}^+\right). \tag{1.7}$$

4. Obtain the finite volume scheme (1.5), then discretize it in time by the TVD Runge-Kutta time discretization [15]. We use the third order version in the numerical tests performed in this paper.

This finite volume scheme is very simple and efficient, and hence is widely used in applications. However, this scheme is only second order accurate for general nonlinear systems (systems in which the physical fluxes $f(u)$ and $g(u)$ are nonlinear functions of u), regardless of the order of accuracy in the one-dimensional reconstruction procedure used in Steps 1 and 2 above. The problem arises in the approximation of the fluxes in Step 3 above, both in the sense of using line averages as inaccurate approximations to the point values in the numerical fluxes and in the sense of inaccurate numerical quadrature. We will give a proof of the second order accuracy of the Class A schemes in the Appendix. Numerical experiments in next section clearly demonstrate this second order accuracy. There is however an important exception. If the system is linear (that is, the physical fluxes $f(u)=Au$ and $g(u)=Bu$, where A and B are constant matrices), such as the linear Maxwell equations and linearized Euler equations, the same high order accuracy as in the one-dimensional reconstruction is achieved, see the Appendix for a proof and next section for numerical verification.

The second class (Class B) of the finite volume methods that we will study in this paper has the following algorithm flowchart:

Finite volume scheme, Class B

1. Using the two dimensional cell averages $\bar{\bar{u}}_{i,j}$, perform a one-dimensional reconstruction procedure in y to obtain a high order accurate approximation to the cell average of u in x at $y = y_{j+1/2}$, denoted by $\bar{u}_{i,j+1/2}$. For the purpose of upwinding and stability, typically two different approximations, denoted by $\bar{u}_{i,j+1/2}^{-}$ and $\bar{u}_{i,j+1/2}^{+}$, based on stencils biased to the left and to the right respectively, are obtained. This step is the same as the first step for the finite volume scheme in Class A.

2. Using the one dimensional cell averages $\bar{u}_{i,j+1/2}^{\pm}$, perform a one-dimensional reconstruction procedure in x to obtain a high order accurate approximation to the point values of u at the Gaussian quadrature points x_i^k, denoted by $u_{i_k,j+1/2}^{\pm}$.

3. Using the two dimensional cell averages $\bar{\bar{u}}_{i,j}$, perform a one-dimensional reconstruction procedure in x to obtain a high order accurate approximation to the cell average of u in y at $x = x_{i+1/2}$, denoted by $\tilde{u}_{i+1/2,j}$. Again, two different approximations, denoted by $\tilde{u}_{i+1/2,j}^{-}$ and $\tilde{u}_{i+1/2,j}^{+}$, based on stencils biased to the left and to the right respectively, are obtained. This step is the same as the second step for the finite volume scheme in Class A.

4. Using the one dimensional cell averages $\tilde{u}_{i+1/2,j}^{\pm}$, perform a one-dimensional reconstruction procedure in y to obtain a high order accurate approximation to the point values of u at the Gaussian quadrature points y_j^k, denoted by $u_{i+1/2,j_k}^{\pm}$.

5. Form the approximate fluxes using the Gaussian quadrature (1.6):

$$\hat{f}_{i+\frac{1}{2},j} = \sum_{k=1}^{q} \beta_k \hat{f}\left(u_{i+\frac{1}{2},j_k}^{-}, u_{i+\frac{1}{2},j_k}^{+}\right), \qquad \hat{g}_{i,j+\frac{1}{2}} = \sum_{k=1}^{q} \beta_k \hat{g}\left(u_{i_k,j+\frac{1}{2}}^{-}, u_{i_k,j+\frac{1}{2}}^{+}\right). \tag{1.8}$$

6. Obtain the finite volume scheme (1.5), then discretize it in time by the TVD Runge-Kutta time discretization [15].

Comparing with the finite volume scheme in Class A, we can observe that the finite volume scheme in Class B is more complicated and more costly, because of the additional reconstructions in Steps 2 and 4 and the Gaussian quadrature sums in Step 5. However, these additional reconstructions and quadratures are necessary to obtain high order approximations to the necessary point values of the solution at suitable quadrature points from the knowledge of two-dimensional cell averages, which are the only information available in a finite volume scheme. The scheme in Class B is genuinely high order accurate for nonlinear systems. We will give a proof of this fact in the Appendix. Numerical experiments in next section clearly demonstrate the high order accuracy.

The focus of this paper is on spatial discretization. We use the same third order TVD Runge-Kutta time discretization for a fair comparison among different spatial discretizations. For more options of time discretization techniques, with improvements in accuracy or efficiency over the third order version used in this paper, we refer to [4].

2 Numerical experiments

We use the two dimensional Euler equations for compressible gas dynamics, namely (1.1) with

$$u = \begin{pmatrix} \rho \\ \rho v \\ \rho w \\ E \end{pmatrix}, \qquad f(u) = \begin{pmatrix} \rho v \\ \rho v^2 + p \\ \rho vw \\ v(E+p) \end{pmatrix}, \qquad g(u) = \begin{pmatrix} \rho w \\ \rho vw \\ \rho w^2 + p \\ w(E+p) \end{pmatrix},$$

where ρ is the density, (v,w) is the velocity, E is the total energy, i.e.,

$$E = \frac{p}{\gamma - 1} + \frac{1}{2}\rho(v^2 + w^2),$$

where p is the pressure, with $\gamma = 1.4$ in our computation. The two classes of finite volume WENO schemes considered in the previous section are compared for accuracy (both linear and nonlinear cases), resolution for shocked solutions, and CPU costs. Time discretization is by the third order TVD Runge-Kutta method [15], with a suitably reduced time step for the accuracy tests so that spatial errors dominate.

In some of the tests we also compare the results with those obtained with a traditional second order TVD scheme [5], which is similar to the Class A scheme except that the reconstructions in Steps 1 and 2 are produced using a piecewise linear polynomial with a minmod limiter, and the time discretization is by the second order TVD Runge-Kutta method in [15]. We use the HLLC numerical flux and do not perform local characteristic decompositions for this scheme. We will refer to this scheme as Class C below. It will be observed that, even though both Class A and Class C schemes are formally second order accurate for nonlinear problems, the results from the Class A scheme are usually much more accurate on the same mesh.

Example 2.1. The initial condition is set to be

$$\begin{cases} \rho(x,y,0) = 1 + 0.5\sin(\pi(x+y)), \\ v(x,y,0) = 1, \\ w(x,y,0) = 1, \\ p(x,y,0) = 1, \end{cases} \tag{2.1}$$

with periodic boundary conditions. The exact solution is

$$\begin{cases} \rho(x,y,0) = 1 + 0.5\sin(\pi(x+y-2t)), \\ v(x,y,0) = 1, \\ w(x,y,0) = 1, \\ p(x,y,0) = 1. \end{cases} \tag{2.2}$$

It is easy to check that, in this special case, the Euler equations actually become a linear system.

Table 1: Example 2.1. L^1 errors and orders of accuracy for density. Class A finite volume scheme.

		Lax-Friedrichs Flux		HLLC Flux	
h	CFL	Error	Order	Error	Order
2/20	0.9	7.31E-04		7.25E-04	
2/40	0.8	2.36E-05	4.95	2.34E-05	4.95
2/80	0.6	7.60E-07	4.96	7.53E-07	4.96
2/160	0.5	2.60E-08	4.87	2.58E-08	4.87
2/320	0.3	7.95E-10	5.03	7.89E-10	5.03

Table 2: Example 2.1. L^1 errors and orders of accuracy for density. Class B finite volume scheme.

		Lax-Friedrichs Flux		HLLC Flux	
h	CFL	Error	Order	Error	Order
2/20	0.9	1.87E-03		7.25E-04	
2/40	0.8	6.12E-05	4.93	2.34E-05	4.95
2/80	0.6	1.94E-06	4.98	7.53E-07	4.96
2/160	0.5	6.28E-08	4.95	2.58E-08	4.87
2/320	0.3	1.95E-09	5.01	7.88E-10	5.03

The computational domain is taken as $[-1,1] \times [-1,1]$. We use uniform meshes with $\Delta x = \Delta y = h$, and give the results with both the Lax-Friedrichs and the HLLC fluxes at time $t = 2.0$ in Tables 1 and 2. Clearly, for this linear system case both classes of the finite volume schemes are fifth order accurate.

This example is often used in the literature to test accuracy of schemes. As we can see here, this is not a stringent test case. The Class A finite volume scheme, which is only second order accurate for general nonlinear problems, easily passes this test as a fifth order scheme.

Table 3: Example 2.1. CPU time (in seconds) for both classes of finite volume schemes.

	Lax-Friedrichs Flux			HLLC Flux		
h	Class A	Class B	Ratio	Class A	Class B	Ratio
2/20	0.41	1.77	4.31	0.46	1.90	4.13
2/40	3.51	15.25	4.34	3.96	16.33	4.12
2/80	36.97	158.51	4.29	41.57	170.32	4.10
2/160	351.63	1504.30	4.28	396.45	1615.41	4.07
2/320	6014.95	20340.81	3.38	6641.45	21856.00	3.29

The CPU time used for both classes of the finite volume WENO schemes is listed in Table 3. Here and below the CPU time is measured on a 1.5GHz Itanium 2 Madison 64 bit CPU. We can see that the Class B finite volume WENO scheme uses about 3 to 4 times more CPU time than the Class A scheme on the same mesh. This is consistent with operation counts of these two classes of schemes (we do not give explicit operation

Table 4: Example 2.1. L^1 errors and orders of accuracy for density, and CPU time (in seconds). CFL=0.8. Traditional second order Class C scheme.

h	Error	Order	CPU time
2/20	5.11E-02		0.16
2/40	2.28E-02	1.16	1.31
2/80	6.70E-03	1.77	10.10
2/160	1.91E-03	1.81	86.55
2/320	5.15E-04	1.89	718.36

counts here to save space; they can be easily obtained from the algorithm flowcharts given in Section 1).

In Table 4, we list the L^1 errors and orders of accuracy for the density and the CPU time used for the traditional second order scheme (Class C). We observe that the CPU time is much smaller than that of either Class A or Class B for the same mesh, but the magnitudes of the error are much larger. For this particular example, to reach an error threshold below 10^{-4}, both Class A and Class B schemes will cost less CPU time than the Class C scheme.

Example 2.2. (2D vortex evolution). This example [13] is a nonlinear example, for which we can observe different orders of accuracy for the two classes of finite volume WENO schemes. The setup of the problem is as following. The mean flow is $\rho = 1$, $p = 1$, $(v,w) = (1,1)$, and the computational domain is $[0,10] \times [0,10]$. We add, to the mean flow, an isentropic vortex, which corresponds to perturbations in (v,w) and the temperature $T = p/\rho$ and no perturbation in the entropy $S = p/\rho^\gamma$:

$$(\delta v, \delta w) = \frac{\varepsilon}{2\pi} e^{0.5(1-r^2)}(-\bar{y}, \bar{x}), \qquad \delta T = -\frac{(\gamma-1)\varepsilon^2}{8\gamma\pi^2} e^{1-r^2}, \qquad \delta S = 0,$$

where $(\bar{x},\bar{y}) = (x-5, y-5)$, $r^2 = \bar{x}^2 + \bar{y}^2$, and the vortex strength $\varepsilon = 5$. Periodic boundary condition is used, which has little effect on the solution since the vortex is close to zero at the initial boundary. It is clear that the exact solution is just the passive convection of the vortex with the mean velocity. The errors at time $t = 0.2$ calculated by the two classes of finite volume WENO schemes are listed in Tables 5 and 6, respectively. We can observe clearly that the accuracy for the Class A finite volume scheme is only second order, while the accuracy for the Class B scheme is fifth order. The errors and orders of accuracy for the traditional second order Class C scheme are listed in Table 7. Even though both Class A and Class C schemes are second order accurate for this example, the error magnitudes of the Class A scheme is much smaller than that of the Class C scheme on the same mesh. In fact, for this particular example, the errors of the Class C scheme with 640^2 cells are larger than that of the Class A scheme with 80^2 cells. This translates to a saving in CPU time even though the Class A scheme is much more expensive than the Class C scheme on the same mesh.

Table 5: Example 2.2. L^1 errors and orders of accuracy for density. Class A finite volume scheme.

h	CFL	Lax-Friedrichs Flux		HLLC Flux	
		Error	Order	Error	Order
10/40	0.8	6.38E-05		5.45E-05	
10/80	0.6	5.24E-06	3.61	4.51E-06	3.60
10/160	0.5	5.81E-07	3.17	5.67E-07	2.99
10/320	0.3	1.38E-07	2.07	1.38E-07	2.04
10/640	0.1	3.46E-08	2.00	3.46E-08	2.00

Table 6: Example 2.2. L^1 errors and orders of accuracy for density. Class B finite volume scheme.

h	CFL	Lax-Friedrichs Flux		HLLC Flux	
		Error	Order	Error	Order
10/40	0.8	7.99E-05		5.39E-05	
10/80	0.6	6.54E-06	3.61	3.98E-06	3.76
10/160	0.5	2.20E-07	4.90	1.20E-07	5.06
10/320	0.3	4.83E-09	5.51	2.69E-09	5.48
10/640	0.1	1.31E-10	5.21	7.44E-11	5.18

Table 7: Example 2.2. L^1 errors and orders of accuracy for density. CFL=0.8. Traditional second order Class C scheme.

h	Error	Order
10/40	6.34E-04	
10/80	2.32E-04	1.45
10/160	8.45E-05	1.46
10/320	2.77E-05	1.61
10/640	8.59E-06	1.69

Example 2.3. We add suitable source terms to the right-hand side of the Euler equations such that the following smooth functions are exact solutions of the resulting nonlinear PDE system

$$\begin{cases} \rho(x,y,t) = 1 + 0.5\sin(\pi(x+y-3t)), \\ v(x,y,t) = \cos(\pi(x+2y+2t)), \\ w(x,y,t) = 1 - 0.5\sin(\pi(2x+y-3t)), \\ p(x,y,t) = 1 + 0.5\sin(\pi(x-y+4t)). \end{cases}$$

The computational domain is $[-1,1]\times[-1,1]$ and periodic boundary condition is applied. The error at time $t=3.0$ calculated by the two classes of finite volume WENO schemes are listed in Tables 8 and 9, respectively. We observe once more that the accuracy for the Class A finite volume scheme is only second order, while the accuracy for the Class B scheme is fifth order. In Table 10, we list the error at time $t=3.0$ calculated by the traditional second order Class C scheme. We again observe that, even though both Class

Table 8: Example 2.3. L^1 errors and orders of accuracy for density. Class A finite volume scheme.

| | | Lax-Friedrichs Flux | | HLLC Flux | |
h	CFL	Error	Order	Error	Order
2/20	0.8	9.72E-02		1.03E-01	
2/40	0.6	9.76E-02	0.00	9.88E-02	0.06
2/80	0.5	3.19E-02	1.61	3.14E-02	1.65
2/160	0.3	8.07E-03	1.98	8.04E-03	1.96
2/320	0.1	2.04E-03	1.98	2.05E-03	1.97

Table 9: Example 2.3. L^1 errors and orders of accuracy for density. Class B finite volume scheme.

| | | Lax-Friedrichs Flux | | HLLC Flux | |
h	CFL	Error	Order	Error	Order
2/20	0.8	9.98E-02		9.68E-02	
2/40	0.6	6.93E-02	0.52	6.15E-02	0.65
2/80	0.5	7.38E-03	3.23	3.66E-03	4.07
2/160	0.3	2.64E-04	4.81	1.11E-04	5.05
2/320	0.1	8.17E-06	5.01	3.43E-06	5.01

Table 10: Example 2.3. L^1 errors and orders of accuracy for density. Traditional second order Class C scheme. CFL=0.8, t=3.0.

h	Error	Order
2/20	1.00E-01	
2/40	1.26E-01	-0.33
2/80	6.58E-02	0.94
2/160	2.50E-02	1.40
2/320	7.41E-03	1.75

A and Class C schemes are second order accurate, the error magnitudes of the Class A scheme is much smaller than that of the Class C scheme on the same mesh.

In Fig. 1, we plot the relationship between the L^1 error of density and CPU time for all classes of schemes in this example. Even though, on the same mesh, the Class B finite volume WENO scheme uses about 3 to 4 times more CPU time than the Class A scheme, and the Class A finite volume WENO scheme uses about 3 to 4 times more CPU time than the traditional second order Class C scheme, to reach a given error tolerance below 2.0×10^{-3}, the Class B scheme uses the least less CPU time, the Class A scheme follows in CPU cost, and the Class C scheme is the most expensive. This is consistent with the general conclusions about high order schemes: they are more economical when high precision simulation is required.

Example 2.4. (Oblique Lax shock tube). The purpose of this test is to assess the capability of the two classes of WENO schemes in resolving waves that are oblique to the computational mesh. The two dimensional Lax problem is solved where the initial jump makes an
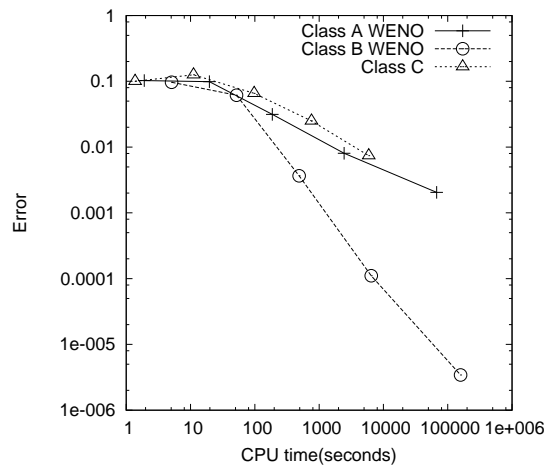
Figure 1: Example 2.3. L^1 error of density versus CPU time for all schemes.

angle θ against x-axis ($0<\theta\leqslant\pi/2$). If $\theta=\pi/2$, we have the one-dimensional Lax problem. If $0<\theta<\pi/2$, all the waves produced will be oblique to the rectangular computational mesh. We take our computational domain to be $[0,14]\times[0,14]$, and $\theta=\pi/4$. The initial jump starts at $(x,y)=(0,0)$. That is, initially we have

$$(\rho,v,w,p)=\begin{cases} \left(0.445,0.698\cos\left(-\tfrac{\pi}{4}\right),0.698\sin\left(-\tfrac{\pi}{4}\right),3.528\right), & \text{if } x<y, \\ (0.5,0,0,0.571), & \text{otherwise.} \end{cases} \tag{2.3}$$

The solution is computed up to $t=1.3$ for the mesh size $\Delta x=\Delta y=1/30$.

We show in Fig. 2 the densities at $y=7$. The solid lines are the exact solution. We can observe that both classes of the finite volume WENO scheme give visually similar results on the same meshes, despite of their different formal order of accuracy.
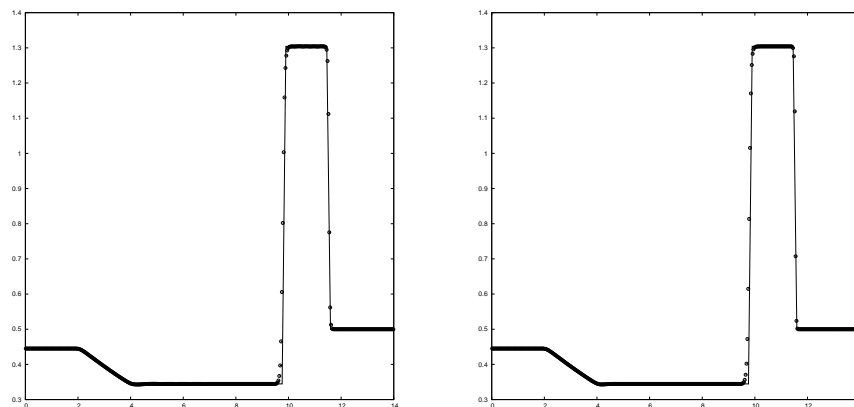

Figure 2: Oblique Lax shock tube. Density at $y=7$. $\Delta x=\Delta y=1/30$, CFL=0.6, HLLC flux. Left: Class A WENO; Right: Class B WENO.
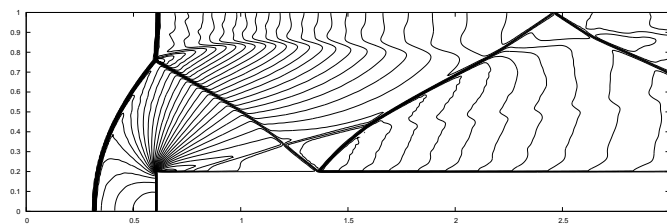
(a) $\Delta x = \Delta y = 1/160$, Class A WENO
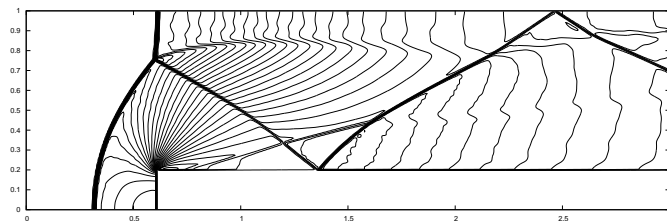
(b) $\Delta x = \Delta y = 1/160$, Class B WENO
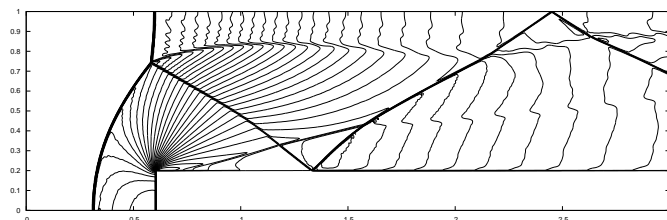
(c) $\Delta x = \Delta y = 1/320$, Class A WENO
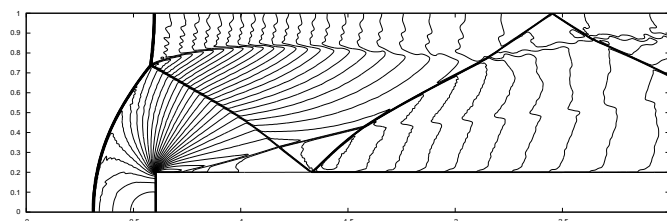
(d) $\Delta x = \Delta y = 1/320$, Class B WENO

Figure 3: Flow past a forward facing step. 30 contours from 0.1 to 6.6, Lax-Friedrichs flux. CFL=0.6.

Example 2.5. (A Mach 3 wind tunnel with a step). This model problem has been carefully examined in Woodward and Colella [17] and later by many others. The setup of the problem is the following. The wind tunnel is 1 length unit wide and 3 length units long. The step is 0.2 length unit high and is located 0.6 length units from the left-hand end of the tunnel. The problem is initialized by a right going Mach 3 flow. Reflective boundary conditions are applied along the walls of the tunnel and in-flow and out-flow boundary

conditions are applied at the entrance (left-hand end) and the exit (right-hand end). For the treatment of the singularity at the corner of the step, we adopt the same technique used in [17], which is based on the assumption of a nearly steady flow in the region near the corner. The numerical results are shown in Fig. 3, for the mesh sizes $\Delta x = \Delta y = 1/160$ and $1/320$. We can observe that both classes of the finite volume WENO scheme give visually similar results on the same meshes, despite of their different formal order of accuracy.

Example 2.6. (Double Mach reflection of a strong shock). The computational domain for this problem is chosen to be $[0,4] \times [0,1]$. The reflecting wall lies at the bottom of the computational domain starting from $x = 1/6$. Initially a right-moving Mach 10 shock

(a) Class A WENO

(b) Class B WENO

(c) Blow-up regions near the Mach stem for details. Left: Class A WENO; Right: Class B WENO
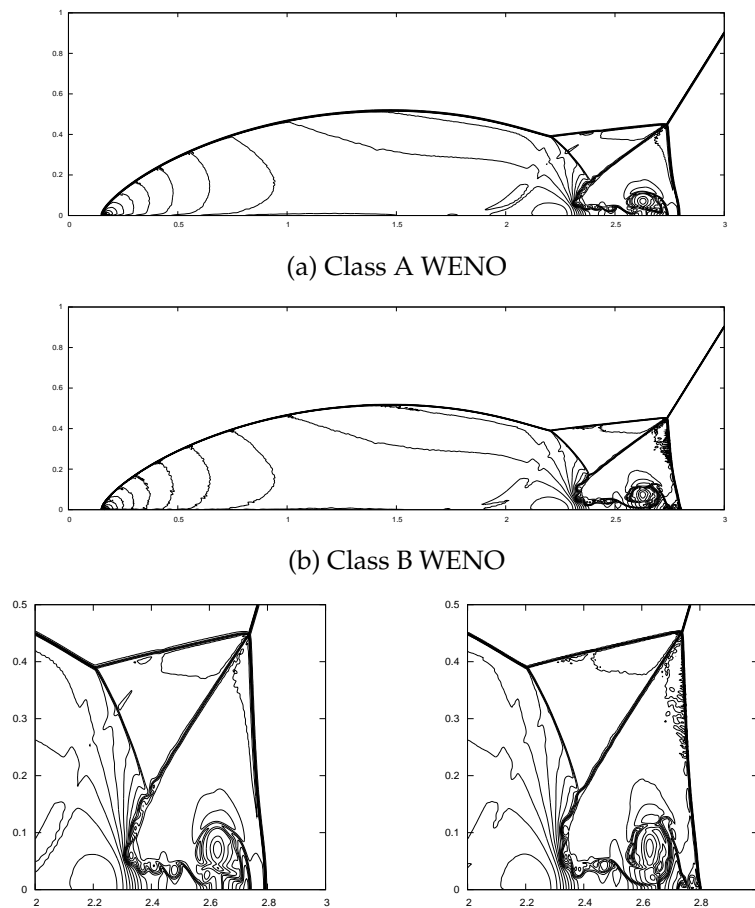
Figure 4: Result for the double Mach reflection. $\Delta x = \Delta y = 1/480$, CFL=0.8, Class A WENO (a) and Class B WENO (b), HLLC flux.
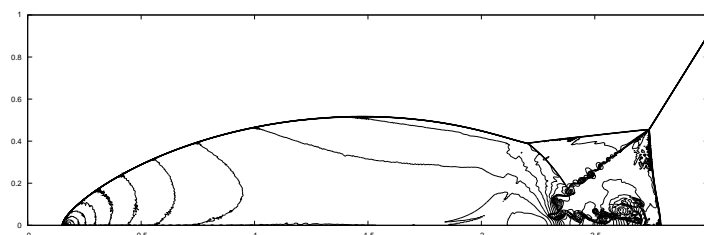
(a) Class A WENO
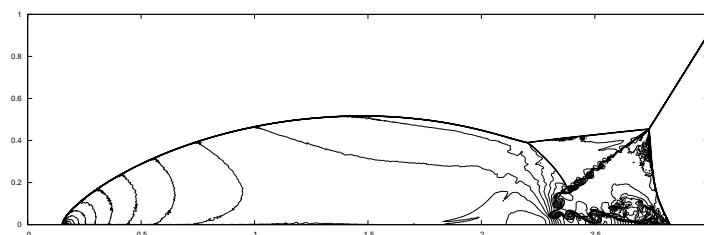
(b) Class B WENO
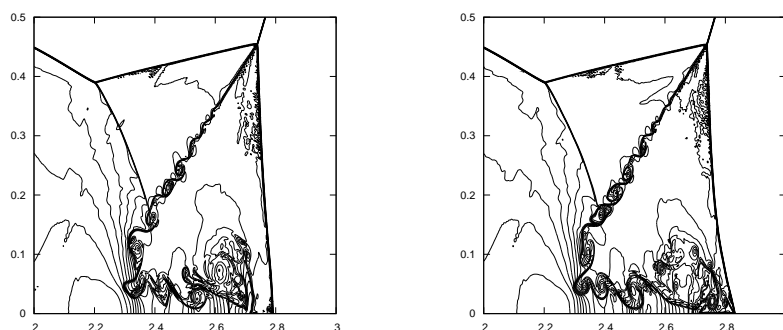
(c) Blow-up regions near the Mach stem for details. Left: Class A WENO; Right: Class B WENO

Figure 5: Result for the double Mach reflection. $\Delta x = \Delta y = 1/960$, CFL=0.8, Class A WENO (a) and Class B WENO (b), HLLC flux.

is positioned at $x = 1/6$, $y = 0$, and makes a 60° angle with the x-axis. For the bottom boundary, the exact postshock condition is imposed for the part from $x = 0$ to $x = 1/6$ and a reflective boundary condition is used for the rest. At the top boundary of our computational domain, the flow values are set to describe the exact motion of the Mach 10 shock. See [17] for a detailed description of the problem.

We give the results of both classes of the finite volume WENO schemes in Fig. 4 with $\Delta x = \Delta y = 1/480$. The results with $\Delta x = \Delta y = 1/960$ are given in Fig. 5. Again, we can observe that both classes of the finite volume WENO scheme give comparable resolutions on the same meshes, despite of their different formal order of accuracy. We also present the results of the traditional second order Class C scheme in Fig. 6. Even though both

(a) $\Delta x = \Delta y = 1/480$

(b) $\Delta x = \Delta y = 1/960$

(c) Blow-up regions near the Mach stem for details. Left: $\Delta x = \Delta y = 1/480$; Right: $\Delta x = \Delta y = 1/960$
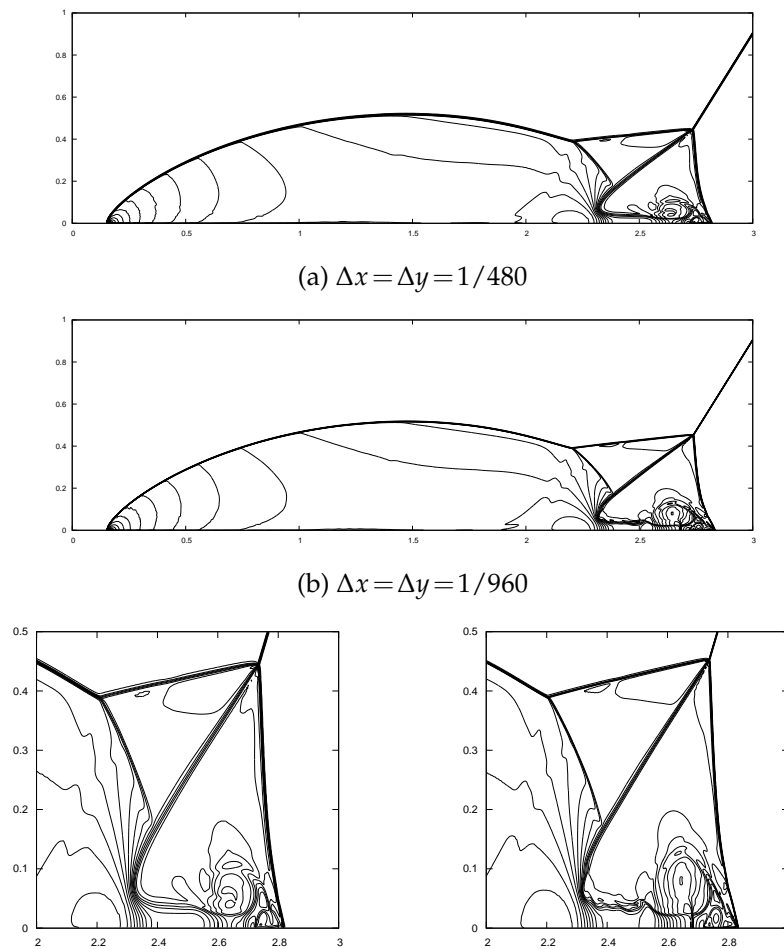
Figure 6: Result for the double Mach reflection. Traditional second order Class C scheme. CFL=0.8. $\Delta x = \Delta y = 1/480$ (a) and $\Delta x = \Delta y = 1/960$ (b).

Class A and Class C schemes are formally second order accurate, it is clear that the Class A result with $\Delta x = \Delta y = 1/480$ is better than that of Class C with the finer mesh $\Delta x = \Delta y = 1/960$, in terms of resolving the "roll-ups" of the slip lines.

3   Conclusions

Two classes of finite volume WENO schemes are discussed and tested in this paper. We observe numerically and prove theoretically that they are both high order accurate for linear systems, however the Class A schemes are only second order accurate for nonlinear systems, while the Class B schemes are still high order accurate. The conclusion holds for

any two point consistent numerical flux, we have tested the Lax-Friedrichs flux and the HLLC flux and have observed no major difference. The operation count and CPU timing for the Class B schemes are about 3 to 4 times of those for the Class A schemes on the same mesh. However, for high precision simulation of smooth flows, Class B schemes could take less CPU time to reach the same error threshold than Class A schemes. For problems with shocks, at least for the test problems that we have experimented in this paper, the two classes of finite volume schemes give comparable resolution on the same meshes, despite of their difference in formal order of accuracy. Results in this paper might shed some light on the popularity of Class A schemes in applications.

We have also performed some comparison with the traditional second order TVD scheme based on piecewise linear reconstructions, termed Class C scheme in Section 2. Even though both Class A and Class C schemes are formally second order accurate for nonlinear problems, the Class A scheme has much more accurate solutions on the same mesh than the Class C scheme. If we would like to reach a low error threshold or to achieve resolution for fine structures in the solution (e.g., to resolve the "roll-ups" of the slip lines in the double Mach reflection problem), the Class A scheme may need less CPU time than the Class C scheme since the former can use a much coarser mesh.

Acknowledgments

Appendix

In this appendix we describe briefly the fifth order WENO reconstruction procedure, and prove the orders of accuracy for the two classes of WENO schemes studied in this paper.

A.1   Fifth order WENO reconstruction

We use the fifth-order WENO reconstruction procedure, described in [8]. Lower or higher order reconstructions are also possible, see for example those in [1,9].

For a piecewise smooth function $v(x)$, we denote $\bar{v}_i$ as its cell average. The fifth-order accurate reconstruction with a left-biased stencil is defined as

$$v^-_{j+\frac{1}{2}} = \omega_0 v_0 + \omega_1 v_1 + \omega_2 v_2, \tag{A.1}$$

where v_k are the reconstructed values obtained from cell averages in the k-th stencil $S_k =$

$(j-k, j-k+1, j-k+2)$:

$$v_0 = \frac{1}{6}(-\bar{v}_{i+2} + 5\bar{v}_{i+1} + 2\bar{v}_i), \tag{A.2a}$$

$$v_1 = \frac{1}{6}(2\bar{v}_{i+1} + 5\bar{v}_i - \bar{v}_{i-1}), \tag{A.2b}$$

$$v_2 = \frac{1}{6}(11\bar{v}_i - 7\bar{v}_{i-1} + 2\bar{v}_{i-2}), \tag{A.2c}$$

and ω_k, $k = 0,1,2$ are the nonlinear WENO weights given by

$$\omega_k = \frac{\alpha_k}{\sum_{l=0}^{2}\alpha_l}, \qquad \alpha_0 = \frac{0.3}{(\varepsilon + IS_0)^2}, \qquad \alpha_1 = \frac{0.6}{(\varepsilon + IS_1)^2}, \qquad \alpha_2 = \frac{0.1}{(\varepsilon + IS_2)^2}. \tag{A.3}$$

Here ε is a small parameter which we take as $\varepsilon = 10^{-6}$ in our numerical tests. We refer also to [7] for a discussion of the effect of ε on the accuracy for various WENO strategies. The smoothness indicators IS_k are given by [8]

$$IS_0 = \frac{13}{12}(\bar{v}_i - 2\bar{v}_{i+1} + \bar{v}_{i+2})^2 + \frac{1}{4}(3\bar{v}_i - 4\bar{v}_{i+1} + \bar{v}_{i+2})^2, \tag{A.4a}$$

$$IS_1 = \frac{13}{12}(\bar{v}_{i-1} - 2\bar{v}_i + \bar{v}_{i+1})^2 + \frac{1}{4}(\bar{v}_{i-1} - \bar{v}_{i+1})^2, \tag{A.4b}$$

$$IS_2 = \frac{13}{12}(\bar{v}_{i-2} - 2\bar{v}_{i-1} + \bar{v}_i)^2 + \frac{1}{4}(\bar{v}_{i-2} - 4\bar{v}_{i-1} + 3\bar{v}_i)^2. \tag{A.4c}$$

The right-biased reconstruction $v_{i+1/2}^+$ is obtained by symmetry with respect to the location $i+1/2$. Reconstructions to values $v(x^*)$ for x^* inside the interval $[x_{i-1/2}, x_{i+1/2}]$ can be obtained along the same lines, in fact only the formulas for the reconstructed values obtained from the small stencils in (A.2) and the linear weights (0.3, 0.6 and 0.1) in (A.3) would change. We refer to, e.g., [10] for more details.

For the systems of conservation laws, a local characteristic decomposition is used in the reconstruction. We refer to [8,13] for more details.

A.2   Accuracy for the two classes of finite volume WENO schemes

Theorem A.1. *The Class B finite volume WENO scheme is accurate to the order of accuracy of the reconstruction and quadrature rules.*

Proof. We take as an example the case of a fifth order reconstruction and three point quadrature rules used in this paper. The proof for the general case is the same. The values $u_{i+1/2,jk}^{\pm}$ at the Gaussian points in (1.8) are reconstructed by the fifth-order WENO procedure, which yields

$$u_{i+\frac{1}{2},jk}^{\pm} = u(x_{i+\frac{1}{2}}, y_j^k) + \mathcal{O}(\Delta x^5 + \Delta y^5), \tag{A.5}$$

where $u(x,y)$ is the exact solution of the PDE (we have suppressed the t variable for simplicity, as we are considering truncation errors in space only). Since the numerical flux $\hat{f}$ is Lipschitz continuous, we have

$$
\begin{aligned}
&|\hat{f}(u^-_{i+\frac{1}{2},jk},u^+_{i+\frac{1}{2},jk})-f(u(x_{i+\frac{1}{2}},y^k_j))|\\
=&|\hat{f}(u^-_{i+\frac{1}{2},jk},u^+_{i+\frac{1}{2},jk})-\hat{f}(u(x_{i+\frac{1}{2}},y^k_j),u(x_{i+\frac{1}{2}},y^k_j))|\\
\leqslant&|\hat{f}(u^-_{i+\frac{1}{2},jk},u^+_{i+\frac{1}{2},jk})-\hat{f}(u^-_{i+\frac{1}{2},jk},u(x_{i+\frac{1}{2}},y^k_j))|\\
&+|\hat{f}(u^-_{i+\frac{1}{2},jk},u(x_{i+\frac{1}{2}},y^k_j))-\hat{f}(u(x_{i+\frac{1}{2}},y^k_j),u(x_{i+\frac{1}{2}},y^k_j))|\\
\leqslant&L\big(|u^+_{i+\frac{1}{2},jk}-u(x_{i+\frac{1}{2}},y^k_j)|+|u^-_{i+\frac{1}{2},jk}-u(x_{i+\frac{1}{2}},y^k_j)|\big)\\
=&\mathcal{O}(\Delta x^5+\Delta y^5).
\end{aligned}
\tag{A.6}
$$

The error for the 3-point Gaussian integration in (1.6) is

$$
\tilde{f}_{i+\frac{1}{2},j}=\sum_{k=1}^{3}\beta_k f(u(x_{i+\frac{1}{2}},y^k_j))+\mathcal{O}(\Delta y^6).
\tag{A.7}
$$

So we can get the error of the flux $\hat{f}_{i+1/2,j}$ in (1.8) as

$$
\tilde{f}_{i+\frac{1}{2},j}=\hat{f}_{i+\frac{1}{2},j}+\mathcal{O}(\Delta x^5+\Delta y^5).
\tag{A.8}
$$

Assuming the leading term in the error $\mathcal{O}(\Delta x^5+\Delta y^5)$ in (A.8) is smooth, we have

$$
\frac{1}{\Delta x}(\tilde{f}_{i+\frac{1}{2},j}-\tilde{f}_{i-\frac{1}{2},j})-\frac{1}{\Delta x}(\hat{f}_{i+\frac{1}{2},j}-\hat{f}_{i-\frac{1}{2},j})=\mathcal{O}(\Delta x^5+\Delta y^5).
\tag{A.9}
$$

Similarly, we have

$$
\frac{1}{\Delta y}(\bar{g}_{i,j+\frac{1}{2}}-\bar{g}_{i,j-\frac{1}{2}})-\frac{1}{\Delta y}(\hat{g}_{i,j+\frac{1}{2}}-\hat{g}_{i,j-\frac{1}{2}})=\mathcal{O}(\Delta x^5+\Delta y^5).
\tag{A.10}
$$

We can see from (A.9) and (A.10) that the local truncation error for the Class B WENO scheme is fifth order. □

Theorem A.2. *The Class A finite volume WENO scheme is second order accurate for general nonlinear conservation laws, but it is accurate to the order of the reconstruction and quadrature rules for linear conservation laws with constant coefficients.*

Proof. The values $\tilde{u}^\pm_{i+1/2,j}$ in (1.7) are reconstructed by the fifth order WENO procedure, hence we have

$$
\tilde{u}^\pm_{i+\frac{1}{2},j}=\tilde{u}_{i+\frac{1}{2},j}+\mathcal{O}(\Delta x^5).
\tag{A.11}
$$

By the Lipschitz continuity of the numerical flux $\hat{f}$, we have

$$
\begin{aligned}
|\hat{f}_{i+\frac{1}{2},j} - f(\tilde{u}_{i+\frac{1}{2},j})| &= |\hat{f}(\tilde{u}^-_{i+\frac{1}{2},j}, \tilde{u}^+_{i+\frac{1}{2},j}) - \hat{f}(\tilde{u}_{i+\frac{1}{2},j}, \tilde{u}_{i+\frac{1}{2},j})| \\
&\leqslant |\hat{f}(\tilde{u}^-_{i+\frac{1}{2},j}, \tilde{u}^+_{i+\frac{1}{2},j}) - \hat{f}(\tilde{u}^-_{i+\frac{1}{2},j}, \tilde{u}_{i+\frac{1}{2},j})| \\
&\quad + |\hat{f}(\tilde{u}^-_{i+\frac{1}{2},j}, \tilde{u}_{i+\frac{1}{2},j}) - \hat{f}(\tilde{u}_{i+\frac{1}{2},j}, \tilde{u}_{i+\frac{1}{2},j})| \\
&\leqslant L\left(|\tilde{u}^-_{i+\frac{1}{2},j} - \tilde{u}_{i+\frac{1}{2},j}| + |\tilde{u}^+_{i+\frac{1}{2},j} - \tilde{u}_{i+\frac{1}{2},j}|\right) \\
&= \mathcal{O}(\Delta x^5).
\end{aligned}
\tag{A.12}
$$

That is

$$
\hat{f}_{i+\frac{1}{2},j} = f(\tilde{u}_{i+\frac{1}{2},j}) + \mathcal{O}(\Delta x^5).
\tag{A.13}
$$

Therefore we have

$$
\frac{\hat{f}_{i+\frac{1}{2},j} - \hat{f}_{i-\frac{1}{2},j}}{\Delta x} = \frac{f(\tilde{u}_{i+\frac{1}{2},j}) - f(\tilde{u}_{i-\frac{1}{2},j})}{\Delta x} + \mathcal{O}(\Delta x^5).
\tag{A.14}
$$

Notice that the cell average of a function agrees with its value at the center of the cell to second order:

$$
\tilde{u}_{i+\frac{1}{2},j} = u(x_{i+\frac{1}{2}}, y_j) + \mathcal{O}(\Delta y^2),
\tag{A.15}
$$

and

$$
\tilde{f}_{i+\frac{1}{2},j} = f(u(x_{i+\frac{1}{2}}, y_j)) + \mathcal{O}(\Delta y^2),
\tag{A.16}
$$

the combination of which gives

$$
f(\tilde{u}_{i+\frac{1}{2},j}) = f(u(x_{i+\frac{1}{2}}, y_j) + \mathcal{O}(\Delta y^2)) = f(u(x_{i+\frac{1}{2}}, y_j)) + \mathcal{O}(\Delta y^2).
\tag{A.17}
$$

We now have

$$
\tilde{f}_{i+\frac{1}{2},j} = f(\tilde{u}_{i+\frac{1}{2},j}) + \mathcal{O}(\Delta y^2),
\tag{A.18}
$$

which is the crucial source of second order error regardless of the order of reconstruction. We have, therefore,

$$
\begin{aligned}
&\frac{1}{\Delta x}(\tilde{f}_{i+\frac{1}{2},j} - \tilde{f}_{i-\frac{1}{2},j}) - \frac{1}{\Delta x}(\hat{f}_{i+\frac{1}{2},j} - \hat{f}_{i-\frac{1}{2},j}) \\
&= \frac{1}{\Delta x}(\tilde{f}_{i+\frac{1}{2},j} - \tilde{f}_{i-\frac{1}{2},j}) - \frac{1}{\Delta x}(f(\tilde{u}_{i+\frac{1}{2},j}) - f(\tilde{u}_{i-\frac{1}{2},j})) + \mathcal{O}(\Delta x^5) \\
&= \frac{1}{\Delta x}(\tilde{f}_{i+\frac{1}{2},j} - f(\tilde{u}_{i+\frac{1}{2},j})) - \frac{1}{\Delta x}(\tilde{f}_{i-\frac{1}{2},j} - f(\tilde{u}_{i-\frac{1}{2},j})) + \mathcal{O}(\Delta x^5) \\
&= \mathcal{O}(\Delta x^5) + \mathcal{O}(\Delta y^2),
\end{aligned}
\tag{A.19}
$$

where $\hat{f}_{i+1/2,j}$ is defined with (1.7).

Similarly,

$$\frac{1}{\Delta y}(\bar{g}_{i,j+\frac{1}{2}}-\bar{g}_{i,j-\frac{1}{2}})-\frac{1}{\Delta y}(\hat{g}_{i,j+\frac{1}{2}}-\hat{g}_{i,j-\frac{1}{2}})=\mathcal{O}(\Delta x^2)+\mathcal{O}(\Delta y^5). \tag{A.20}$$

From (A.19) and (A.20), we can see that the scheme is only second order accurate.

Now, if $f(u)=Au$ is linear, then

$$\int_{y_{j-\frac{1}{2}}}^{y_{j+\frac{1}{2}}} f(u(x_{i+\frac{1}{2}},y))dy=f\Big(\int_{y_{j-\frac{1}{2}}}^{y_{j+\frac{1}{2}}} u(x_{i+\frac{1}{2}},y)dy\Big), \tag{A.21}$$

that is, instead of (A.18) we now have

$$\tilde{f}_{i+\frac{1}{2},j}=f(\tilde{u}_{i+\frac{1}{2},j}), \tag{A.22}$$

thereby avoiding the crucial second order error. From (A.19), we can then get

$$\frac{1}{\Delta x}(\tilde{f}_{i+\frac{1}{2},j}-\tilde{f}_{i-\frac{1}{2},j})-\frac{1}{\Delta x}(\hat{f}_{i+\frac{1}{2},j}-\hat{f}_{i-\frac{1}{2},j})=\mathcal{O}(\Delta x^5), \tag{A.23}$$

which leads to fifth order in the local truncation error for this linear case.   □

References

[1] D. S. Balsara and C.-W. Shu, Monotonicity preserving weighted essentially non-oscillatory schemes with increasingly high order of accuracy, J. Comput. Phys., 160 (2000), 405–452.

[2] R. Borges, M. Carmona, B. Costa and W. S. Don, An improved weighted essentially non-oscillatory scheme for hyperbolic conservation laws, J. Comput. Phys., 227 (2008), 3191–3211.

[3] J. Casper, C.-W. Shu and H. L. Atkins, Comparison of two formulations for high-order accurate essentially nonoscillatory schemes, AIAA J., 32 (1994), 1970–1977.

[4] S. Gottlieb, D. I. Ketcheson and C.-W. Shu, High order strong stability preserving time discretizations, J. Sci. Comput., 38 (2009), 251–289.

[5] A. Harten, High resolution schemes for hyperbolic conservation laws, J. Comput. Phys., 49 (1983), 357–393.

[6] A. Harten, B. Engquist, S. Osher and S. Chakravarthy, Uniformly high order essentially non-oscillatory schemes, III, J. Comput. Phys., 71 (1987), 231–303.

[7] A. K. Henrick, T. D. Aslam and J. M. Powers, Mapped weighted essentially non-oscillatory schemes: achieving optimal order near critical points, J. Comput. Phys., 207 (2005), 542–567.

[8] G.-S. Jiang and C.-W. Shu, Efficient implementation of weighted ENO schemes, J. Comput. Phys., 126 (1996), 202–228.

[9] X.-D. Liu, S. Osher and T. Chan, Weighted essentially non-oscillatory schemes, J. Comput. Phys., 115 (1994), 200–212.

[10] Y.-Y. Liu, C.-W. Shu and M. Zhang, On the positivity of linear weights in WENO approximations, Acta. Math. Appl. Sinica., 25 (2009), 503–538.

[11] J. Qiu, B. C. Khoo and C.-W. Shu, A numerical study for the performance of the Runge-Kutta discontinuous Galerkin method based on different numerical fluxes, J. Comput. Phys., 212 (2006), 540–565.

[12] S. Serna and A. Marquina, Power ENO methods: a fifth-order accurate weighted power ENO method, J. Comput. Phys., 194 (2004), 632–658.

[13] C.-W. Shu, Essentially non-oscillatory and weighted essentially non-oscillatory schemes for hyperbolic conservation laws, in Advanced Numerical Approximation of Nonlinear Hyperbolic Equations, B. Cockburn, C. Johnson, C.-W. Shu and E. Tadmor (Editor: A. Quarteroni), Lecture Notes in Mathematics, Volume 1697, Springer, Berlin, 1998, 325–432.

[14] C.-W. Shu, High order weighted essentially non-oscillatory schemes for convection dominated problems, SIAM Rev., 51 (2009), 82–126.

[15] C.-W. Shu and S. Osher, Efficient implementation of essentially non-oscillatory shock-capturing schemes, J. Comput. Phys., 77 (1988), 439–471.

[16] E. F. Toro, Riemann Solvers and Numerical Methods for Fluid Dynamics, A Practical Introduction, Springer, Berlin, 1997.

[17] P. Woodward and P. Colella, The numerical simulation of two-dimensional fluid flow with strong shocks, J. Comput. Phys., 54 (1984), 115–173.

[18] W. Zhang and A. MacFadyen, RAM: a relativistic adaptive mesh refinement hydrodynamics code, Astrophys. J. Supp. Ser., 164 (2006), 255–279.